A biomimetic robot for tracking specific odors in turbulent plumes

Dominique Martinez, Oliver Rochel and Etienne Hugues

LORIA, Campus Scientifique - BP 239

54506 Vandoeuvre-Les-Nancy, France

Phone: +33 383-59-30-72

Fax: +33 383-41-30-79

Abstract

Two basic tasks must be performed by an olfactory robot tracking a specific odor source : navigate in a turbulent odor plume and recognize an odor regardless of its concentration. For these two tasks, we propose simple biologically inspired strategies, well suited for building dedicated circuits and for on-board implementation on real robots. The odor recognition system is based on a spiking neural network using a synchronization coding scheme. The robot navigation system is based on the use of bilateral comparison between two spatially separated gas sensors arrays at either side of the robot. We propose binary or analog navigation laws depending on the nature

of the available sensory information extracted from the plume structure (isolated
odor patches or smoother concentration field).

1   Introduction

The localization of a specific odor source with a robot equipped with gas sensors is a dif-
ficult task (Ishida and Moriizumi, 2003). Because of the slowness of the diffusion process,
the majority of odorant fields encountered naturally are mainly due to the advection trans-
port, and are furthermore turbulent, the medium being gaseous or liquid. In the case of
turbulence, the concentration landscape of an odor, called a plume, is very heterogenous
and unsteady, and consists of sporadically located patches (Weissburg, 2000; Roberts and
Webster, 2002). These patches move with the local wind and are continuously mixed with
other patches containing odors from different sources. Because gas sensors are non-selective
and respond to a wide variety of gases, an olfactory robot may locate a source that is dif-
ferent from the one of interest. In order to track a specific odor source, two basic tasks
must be performed by an autonomous robot : navigate in a turbulent plume and recognize
the odor independent of its concentration. The goal of this paper is to propose biologically
inspired strategies for performing these two tasks

Recent experimental measures using laser-induced-fluorescence (Webster and Weissburg,
2001; Webster et al., 2001; Weissburg et al., 2002) have given a more accurate view of
the concentration field characteristics in the case of uniform advection. Although con-

centration fluctuations are very high, a steady picture of the field can be obtained by averaging the instantaneous fluctuations within a temporal window of about 200 sec. The resulting averaged concentration field looks very similar to a laminar advection-diffusion profile (Webster and Weissburg, 2001). Furthermore, it has been shown that the probability to find a concentration higher than that at the centerline rapidly decreases with the lateral distance from the centerline (Webster et al., 2001). Some animals could therefore use the instantaneous bilateral comparison of their spatially separated chemosensors to make tracking decisions. This hypothesis is supported by recent experiments showing that unilateral lesions in some animals, e.g. the blockage of the nasal air flow in one nostril in rats or the ablation of one of the antennae in crayfish, impair odor source localization (Kraus-Epley and Moore, 2002; Rajan et al., 2006; McMahon et al., 2005).

Like artificial gas sensors, a biological olfactory sensory neuron is not tuned to a specific odor (Duchamp-Viret et al., 1999). Because the variety of receptor proteins underlying chemoreception is not as rich as the repertoire of existing odorant molecules, different molecules may react with a particular protein and, thus, non-selectivity is probably an unavoidable situation an olfactory system has to face. This problem is still a challenge for electronic noses, as no really satisfactory general solution for improving both the sensitivity and the selectivity has been proposed so far. Understanding how early biological systems encode olfactory sensory information could then be highly beneficial for designing efficient electronic noses. Recent electrophysiological recordings in the mouse olfactory bulb have shown that the phase of the firing of a principal neuron relative to the beginning

of each respiration cycle reflects input intensity (Margrie and Schaefer, 2003). Moreover, this experimental work, as well as a theoretical one (Hopfield, 1995), shows an approximate logarithmic relationship between firing latency and odor intensity. Such a logarithmic function makes the phase pattern invariant to the different concentrations of the same odor. When the odor concentration changes, the entire phase pattern is shifted but the relative phases are preserved. Reading the relative phase pattern can be accomplished in a biological plausible way with delay lines and synchronization detector neurons (Hopfield, 1995; Lysetskiy et al., 2002).

In this paper, the above ideas are exploited for developing a biomimetic robot capable of tracking specific odor sources in turbulent plumes. To recognize an odor independent of its concentration, a bio-inspired algorithm is derived in section 3.1. To navigate in a turbulent plume, a guidance of the robot based on bilateral comparison is proposed in section 3.2.

2 Materials

Our olfactory robot consists of a Koala robot from k-team[1] with an on-board computer (PC104 running Linux) and two electronic noses (E-noses) placed on either side of the robot (see Fig. 1-A). In order to limit corruption of the data due to an additional airflow created by the movement of the robot, two inlet pipes (sniffers) allow to sample the surrounding atmosphere in front of the robot (at the left and at the right). Two pumps (Diaphragm

[1]www.k-team.com

4

pumps SERCOM 2002 0.35 l/min) then feed the gas directly to the sensors in each E-nose. Data multiplexing (Multiplexer CD74HCT4052E from Texas Instrument), acquisition and processing is performed on the robot. The sampled sensor readings are amplified (Amplifier LMC6462 from National Semiconductor) and quantized with the analog to digital converter available on the koala robot from k-team (6 analog inputs, 10 bits of resolution, 4.096 volts of dynamic range). The gain of the amplifier is automatically adjusted online during the experiments so as to make a full use of the quantization range. One particular gain among four fixed available gain levels (x1, x2, x4, x8) is selected at each sampling period (0.1 second) based on a simple threshold-crossing procedure.

Each electronic nose consists of a closed plexiglas chamber that encompasses a sensor array (see Fig. 1-B). The sensor array is composed of ten gas sensors divided into five different types (Figaro TGS 2600, 2602, 2610, 2611 and 2620). These sensors are commercialized with a cap that has a flame-proof stainless steel gauze. In practice, it takes a certain time for the gas to diffuse through the gauze and reach the sensor. This cap was removed from all the sensors (see Fig. 1-C). It improves their response time by a factor ten (see Fig. 2). Calibration of the electronic noses has been done for ethanol and butanol vapors of concentrations ranging from 700 to 3000 ppm at a room temperature of 23^0C. In order to extract volatile compounds at given concentrations from liquids, an automated gas delivery experimental setup was developed (see Fig. 3). Note that this setup is needed for the *calibration method 1* only (it is not for the *calibration method 2*, see calibration methods in section 3.1).

The navigation experiments were performed in an arena of 240 cm long by 120 cm large.

An ethanol source was placed at $x = 240$ cm and $y = 90$ cm and released at a low rate of 0.35 l/min (see Fig. 4). To get a turbulent plume, advection is created by a fan (Papst fan 3412 NL 12 VDC 61 m^3/h) placed just behind the source.

3 Methods

3.1 Bio-inspired odor recognition

Odor recognition method - The steady state change in conductance, x_{ij} of a metal-oxide gas sensor i to an odor j of concentration C_j is known to vary in a non-linear way (power law) with gas concentration (Gardner and Bartlett, 1999)

$$x_{ij} = \alpha_{ij} \, C_j^{r_{ij}} \tag{1}$$

where α_{ij} and r_{ij} are coefficients that depend upon the odor and the sensor. Let us consider a neural network with spiking neurons such that, when an odor k is sampled at time $t = 0$, the input neuron i (connected to sensor i) will fire its first spike at time t_{ik} given by

$$t_{ik} = (\log x_{ik})/r_{ij} \tag{2}$$

where x_{ik} is the steady state change in conductance of sensor i and r_{ij} is the parameter fitted in Eq. 1 for odor j. Additionally, the delay of connection between the input neuron i and the output neuron was set to

$$\Delta_{ij} = \Delta - (\log \alpha_{ij})/r_{ij} \tag{3}$$

where Δ is a constant taken as $\max\{(\log \alpha_{ij})/r_{ij}\}$ in order to preserve causality. If the odor k corresponds to the odor j we want to detect, then $x_{ik} = x_{ij}$ and the spike fired by the input neuron i will arrive at the output neuron at time

$$t_{ij} + \Delta_{ij} = \Delta + \log(C_j) \tag{4}$$

which is independent of the neuron i. Therefore, in presence of odor j, all the spikes fired by the input neurons will arrive at the same synchronization time given by Eq.4. Moreover, in presence of another odor k different to j, the spikes will arrive at unsynchronized times. Given a suitable set of connection delays, spike synchronization will occur in the presence of odor j only, and for any concentration of this particular odor. In this scheme, the connection delays represent a prototype pattern of the odor to be detected.

Calibration methods - In order to set appropriate connection delays, the electronic noses need to be calibrated. The *Calibration method 1* consists in estimating parameter α_{ij} and r_{ij} by fitting real data with the power law given by Eq. 1. The *Calibration method 1* requires the use of an automated gas delivery experimental setup with control of the gas concentration (see Fig. 3). In order to avoid the need of such an olfactometer we can use a given sensor as a reference, say sensor 1 without loss of generality. Using Eq. 1, we can write

$$\log x_{ij} = a_{ij} \log x_{1j} + b_{ij} \tag{5}$$

with $a_{ij} = r_{ij}/r_{1j}$ and $b_{ij} = \log \alpha_{ij} - a_{ij} \log \alpha_{1j}$. In presence of an odor k, we now consider

that the input neuron i fires at

$$t_{ik} = (\log x_{ik})/a_{ij} \qquad (6)$$

and that the connection delay to the output neuron is

$$\Delta_{ij} = \Delta - (b_{ij}/a_{ij}) \qquad (7)$$

If the odor k corresponds to the odor j we want to detect, then $x_{ik} = x_{ij}$ and the spikes fired by the input neurons will arrive at the output neuron at the same time $\log x_{1j} + \Delta = r_{1j}\log(C_j) + \Delta + \log \alpha_{1j}$. Parameters a_{ij} and b_{ij} needed to set the appropriate synaptic delay Δ_{ij} are now identified by fitting real data of sensor i versus sensor 1 with Eq. 5 (*Calibration method 2*). Thus, the *Calibration method 2* does not require the explicit knowledge of the concentration C_j.

3.2   Navigation laws based on bilateral comparison

We consider here the navigation of our robot with two spatially separated sensor arrays. Let $C_l(t)$ and $C_r(t)$ be the odor concentrations estimated at time t by the sensors at the left and at the right, respectively. The concentration difference $C_l(t) - C_r(t)$ is noted $\Delta C(t)$. Because we need to have a high manoeuvrability allowing the robot to turn quickly when it goes out of the plume, we decided to control the turning speed ω and let the velocity v of the robot constant. This allows to control the trajectory via its curvature radius $R = v/\omega$. We propose binary or analog navigation laws depending on the nature of the available sensory information : in the binary case, only the side of the highest concentration is known,

while in the analog case the graded concentration levels at both sides are known.

Binary bilateral comparison - Due to the turbulent nature of odor plumes, the information available might be binary only, indicating whether an odor patch hits the left or the right sensor. When only the side hitted by an odor patch is known, the simplest navigation law based on binary bilateral comparison would be

$$\omega(t) = \Omega(t) \ \mathrm{sgn}(\ \Delta C(t) \ )$$

If $\Omega(t) = \Omega_0$ where Ω_0 is some constant turning speed, we obtain simple circular trajectories whose radius is $R_0 = v/\Omega_0$. Convergence is however dependent on a particular choice for Ω_0. On the one hand, large Ω_0 is needed when the orientation of the robot is far from the optimum so that it can turn sufficiently quickly to reach the centerline of the plume. On the other hand, a small Ω_0 is needed when the orientation of the robot is at the optimum so as to avoid large amplitude oscillations around the centerline of the plume. To circumvent this problem, we propose to make Ω adaptive using the following heuristic rule : if ΔC does not change sign between two consecutive hits, we consider that the current orientation of the robot is far from the optimum. Ω is then multiplied by $\Lambda > 1$ ($\Lambda = 1.1$ here). If ΔC changes sign between two consecutive hits, we consider that the current orientation of the robot is near the optimum and thus Ω is divided by Λ. This gives

$$\begin{aligned} \Omega(t) \ &= \ 1.1 \ \Omega(t - \Delta t) \ \text{if} \ \Delta C(t) = \Delta C(t - \Delta t) \\ &= \ 0.9 \ \Omega(t - \Delta t) \ \text{otherwise} \end{aligned} \tag{8}$$

where Δt is the sampling period.

Analog bilateral comparison - In case we have access to a graded information concerning the lateral concentrations, we have previously considered the navigation laws $\{\mathcal{L}_n\}_{0 \leq n \leq 1}$

$$\omega(t) = \Omega_0 \, \mathrm{sgn}(\, \Delta C(t) \,) \, \mid \Delta C(t) \mid^n \, \bar{C}(t)^{1-2n} \tag{9}$$

$\bar{C} = (C_l + C_r)/2$ is the average concentration and n is a parameter to be specified, where $0 \leq n \leq 1$ to insure convergence in case of an axisymmetric concentration field (Hugues et al., 2003).

Simulations - In the simulation of the navigation laws, time is discretized as in real experiments. This time discretization may induce some instabilities when navigating near the source, but it was found that they could be avoided by decreasing the distance covered by the robot between two measurements. All the navigation laws were first evaluated in two situations : -axisymmetric- diffusion and advection-diffusion. A gaussian plume model derived from the advective-diffusion equation was used (Roberts and Webster, 2002). In the model, the diffusion coefficient of the gas and the air velocity along direction x have been chosen so as to get profiles along direction y as large as in the real turbulent experiments (Hugues et al., 2003). Two noisy conditions were considered so as to take turbulence into account :

NC1) a uniform multiplicative noise with standard deviation σ was applied to C_l and C_r. To simulate a similar level of noise as the actual one in the experiments, but somewhat

higher to judge the efficiency of these laws, a value of $\sigma = 0.2$ was chosen.

NC2) C_l and C_r were inverted randomly with probability p and the lowest concentration was set to zero in order to mimic the fact that an odor patch has reached only one side of the robot. In the simulations performed, $p = 0.3$ was chosen.

4 Results

4.1 Concentration invariant odor recognition

Figure 5 shows the steady state responses R_s/R_o of the 10 sensors with respect to the concentrations in butanol (15 different concentrations). R_s and R_o is the resistance obtained in presence of the gas and the air, respectively. In each plot, the curve representing the power law obtained with the fitted parameters α_{ij} and r_{ij} is also indicated. These fitted parameters are necessary for setting the connection delays by using Eq. 3 in the *Calibration method 1*. The set of delays then represents a prototype pattern of the gas to be detected (here butanol). A match between this prototype pattern and the current odor leads to spike synchronization and thus recognition.

Using the butanol connection delays, we now consider a spiking neural network with 10 input neurons and a single output neuron as a butanol detector. Each input neuron is connected to a single sensor and fires a spike at a time given by Eq. 2 if the *Calibration method 1* was used to estimate the model parameters or by Eq. 6 if the *Calibration method 2* was used. These spikes are received by the output neuron after some delays given by

Eq. 3 or Eq. 7, depending on the method of calibration. Figure 6 shows the arrival times of the spikes for increasing concentrations of butanol and ethanol. In this experiment, the *Calibration method 1* was used. When the odor concentration changes, the entire phase pattern is shifted but synchronization is preserved for butanol. For the different concentrations considered, spike synchronization is better for butanol than for ethanol, by using the butanol connection delays.

In order to compare the results, we have estimated the model parameters for the two E-noses on the robot with the Calibration method 1 and 2, and for the butanol and ethanol detectors. Fig. 7 shows the temporal jitter of the received spikes in the different cases (left or right E-nose, ethanol or butanol detector, calibration method 1 or 2). For each E-nose, the temporal jitter of the received spikes for the butanol detector is higher for ethanol than for butanol, and vice versa for the ethanol detector. It means that discrimination between butanol and ethanol is accomplished at these concentration levels by using an output neuron acting as a synchronization detector. Moreover, the two different calibration methods lead to similar results. The *calibration method 2* is however preferable because of its simplicity (no need of the olfactometer).

4.2   Navigation laws

Simulation results - Simulations of the binary navigation law in the laminar situations show a very good efficiency (data not shown). In the simulated airflow using the noisy conditions NC1 and NC2, the efficiency is still good, apart the appearance of wandering

behaviors illustrated here by loops (see figure 8-A and 9-A).

In the case of the analog navigation laws, $\mathcal{L}_0$ cannot always allow the convergence to the source because the term $\bar{C}$ appearing in it is too small when the robot is far from the source (see figure 8-B). For the noisy condition NC2, it actually never converges (see figure 9-B). For strong noise, $\mathcal{L}_1$ is no longer efficient as the robot turns too much far from the source, due to the term $1/\bar{C}$ appearing in it (see figure 8-D and 9-D). All other laws in the family $\{\mathcal{L}_n\}_{0 \leq n \leq 1}$ 'interpolate' between the two preceding cases, and among them, we have chosen $\mathcal{L}_{1/2}$, which is furthermore independent of $\bar{C}$. This law appears to be the most efficient in the two noisy conditions (see figure 8-C and 9-C).

Experimental results - The spatial distribution of the sensor responses in presence of the released ethanol gas has been obtained by scanning the arena with the robot moving at 2.5 cm/sec. The contour map of this distribution, shown in figure 10 left, demonstrates that a concentration gradient information can be extracted with our gas sensing system, and when the robot is moving at a relatively low speed. One important point to note here is that, in the case of robots, the measurement system -or electronic nose (see (Gardner and Bartlett, 1999; Pearce et al., 2003))- generally filters out, up to the scale of several seconds, the fastest concentration fluctuations. This filtering comes mainly from the slowness of the sensors responses as compared to the steepness of turbulent fluctuations. This fact has been clearly shown in (Yamanaka et al., 1998) for metal-oxide sensors. Thus, a robot equipped with such sensors navigates in an apparent much weaker turbulent odor plume, in which isolated patches are replaced by a smoother concentration field which fluctuates

around a non-zero mean, as shown in figure 10 left. Therefore, when the real turbulent flow has a concentration gradient which varies sharply in space and time due to the presence of patches, this 'apparent' plume has a gradient direction which evolves on a sufficiently large scale to allow its evaluation using two distant sensor arrays.

Because, in case of our robot, the nature of the available sensory information is analog, we report here results for the $\mathcal{L}_{1/2}$ law. The two sensor arrays were first calibrated so that the robot moves straight ahead in presence of a null concentration gradient obtained when the same information was simultaneously fed to the two arrays. Over 16 runs performed with the robot starting from the same location ($x = 70$ and $y = 70$) inside the plume, 13 have successfully converged to the source location. Some of these trajectories are depicted in figure 10 right. The trajectories were obtained using the available data from the odometers on the robot, using a simple dead reckoning approach to estimate the global position at each point in time. The fact that the trajectories differ is due to the fluctuating character of the field. The few unsuccessful runs can be explained by the fact that the robot moved sometimes in a wrong direction due to the turbulent nature of the odor plume. Because the size of the arena was small we were not able to see if the robot might have been able to correct it afterwards. However, if the robot leaves the plume by chance then it will continue to move straight and never returns because the sensory signal outside the plume is weak. This was clearly seen when the robot has started searching from the location $x = 200$ and $y = 20$. As this starting point is outside the plume, concentration levels are extremely small (see the quantized values in the contour plot in Fig. 10 left) and the success rate was very low. In such cases, an exploration strategy is therefore needed but

this is out of the scope of the present paper.

Figure 11 shows the mean sensor reading with respect to the distance to the source during the successful robot trajectories. The mean sensor reading is obtained by averaging the outputs of the sensors (quantized with 10 bits) from the E-noses at the left and the right sides of the robot. The maximum of the sensor reading is not obtained at the source location but at 20 ± 9 cm from the source, in agreement with the contour plot in Fig. 10 left. Two types of trajectories have been found, those for which the sensor reading increases during the path towards the source (figure 11 at the left) and those for which the sensor reading does not always increase (figure 11 at the right). Because the wind is in the x-direction, the concentration drops very fast in the y-direction, and the sensed chemical concentration is not always a useful indicator of distance to the source. Therefore, a strategy purely based on climbing a concentration gradient may fail because the concentration gradient is larger in the y-direction than in the x-direction.

5   Discussion

There exist previous works about autonomous olfactory robots capable of searching for an odor source (Ishida and Moriizumi, 2003). In the simplest case of diffusion, Porat and Nehorai (1996) derived a statistical estimator for the odor source location. Russel (1999) investigated odor trail marking and following by mobile robots. In the case of turbulence, the situation is however more complicated, as the odor plume consists of discontinuous odor patches moving with the local wind. The olfactory sensory information available

15

might thus be binary only, indicating whether an odor patch hits the sensor. Because of the poor olfactory information, a classical approach is to use additional sensory cues provided by the speed and the direction of the wind. Hayes et al. (2002) implemented on a real robot an algorithm that merely uses the binary information given by the presence or the absence of an odor patch to decide either to move the robot upwind or to perform a local search. This algorithm is similar to the one developed by Balkovsky and Shraiman (2002) who considered a simplified model of a turbulent plume based on a random walk of odor patches. In addition to gas sensors, the implementation of navigation laws based on the direction of the wind requires the use of an anemometer. However, because of the relative imprecision of the anemometers that can be used on real robots, this approach is only valid in presence of a strong airflow, as noted in (Lilienthal and Duckett, 2003). Instead, we proposed in this paper the use of bilateral comparison between two spatially separated gas sensor arrays to estimate the direction from which the odor patch came. The idea of using bilateral odor sampling on a real robot is motivated both by physical measurements on natural plumes (Webster and Weissburg, 2001; Webster et al., 2001; Weissburg et al., 2002) and by biological experiments on animal behavior (Kraus-Epley and Moore, 2002; Rajan et al., 2006; McMahon et al., 2005).

Previous works about autonomous olfactory robots using bilateral comparison include the robotic 'lobster' for tracking saline plumes in water from Grasso and Colleagues (Consi et al., 1995; Grasso et al., 1997; Grasso, 2001) and the Braitenberg olfactory robot from Lilienthal and Duckett (2003). The fundamental aspect of these studies is the fact that

16

the sensed olfactory information is analog. In this paper, we have proposed and studied several navigation laws depending on the nature of the available sensory information extracted from the plume structure (isolated odor patches or smoother concentration field). Due to the limited amount of sensory information required, the binary navigation law (Eq. 8) appears to be well suited to a turbulent situation made of intermittent isolated odor patches. The binary navigation law was very efficient in simulation (see Fig. 8A and 9A). Convergence comes from the fact that the probability to find an odor patch rapidly decreases with the lateral distance from the centerline (Webster et al., 2001). In the case of our robot, the gas sensing system filters out, up to the scale of several seconds, the fastest concentration fluctuations. A faster measurement system giving us access to isolated odor patches would then be needed to test the binary navigation law in practice. In our experiments, the robot moves at a low speed (2.5 cm/sec) so that a concentration gradient information can be extracted with our gas sensing system (see Fig. 10 left). Because of the graded nature of the sensory information available, the analog navigation law $\mathcal{L}_{1/2}$ (Eq. 9 with $n = 0.5$) was implemented on our robot and successfully tested in presence of a chemical odor plume (see Fig. 10 right, some videos of the experiments are available at http://www.loria.fr/~dmartine/videos). Over 16 runs performed with the robot starting from the same location inside the plume, 13 have successfully converged to the source location. However, if the robot starts outside the plume or if it leaves the plume, then it will continue to move straight and never returns because the sensory signal outside the plume is weak. This is consistent with previous observations made by others, e.g. in (Consi et al., 1995). When the robot is outside the plume, an exploration strategy is needed, for example

17

by using a zigzag or a spiral trajectory (Hayes et al., 2002; Balkovsky and Shraiman, 2002). In agreement with previous works, e.g. (Lilienthal and Duckett, 2003), we found that the maximum of the sensor reading is not obtained at the source location but at 20 ± 9 cm from the source (see Fig. 10 left or Fig. 11). As distance from the source increases, the odor plume tends to spread both horizontally and vertically. Nevertheless, close to the source, the plume has a limited height. Because the gas sensors on the robot cannot be designed to be exactly at the same (unknown) altitude than the odor source, the chemical concentration sampled near the source does not always match the distance to the source. A better estimation of the source location could have been obtained by rotating the robot at the location of the maximum and using a series of measurements, as in (Nakamoto et al., 1996; Ishida et al., 1999; Lilienthal et al., 2004).

While navigating inside the plume, the robot encounters odor patches of various concentrations. Recognizing an odor regardless of its concentration is therefore a basic task that is needed for tracking specific sources. For this goal, we have proposed a simple biologically inspired spiking neural network using a synchronization coding scheme. The connection delays represent a prototype pattern of the odor to be detected. A match between this prototype pattern and the current odor leads to spike synchronization and thus recognition. When the odor concentration changes, the entire firing pattern is shifted but synchronization is preserved. In order to set appropriate connection delays, two calibration (or training) methods were proposed, a first one that requires the use of an olfactometer with control of the gas concentration, and a second one which does not. This scheme was

successfully tested on a discrimination task between butanol and ethanol with the two electronic noses mounted on the robot. The two different calibration methods lead to similar results. The second calibration method is however the only one that can be implemented on a real robot because of its simplicity, the parameters being just identified by a linear fit from several measurements without requiring knowledge of the odor concentration (see Eq. 5). To the best of our knowledge, there exist a single work performing odor recognition on an olfactory robot, by using a multilayer neural network (Marques et al., 2002). However, the training procedure is complex, time-consuming and, thus, difficult to implement on a real robot. Instead, due to its simplicity, our odor recognition spiking neural network is particularly well suited for building dedicated VLSI circuits and/or for on-board implementations on real robots. When the robot moves continuously, the steady state of the sensor responses may not be available but can be predicted from the transient response, as shown in (Yamanaka et al., 1998).

As mentioned above in the discussion, future work is still necessary as extensions to this research. In particular, work is ongoing to test the binary navigation law with two simultaneous, different odor plumes, where the robot is required to both identify and locate one of the odor sources.

Acknowledgments

References

Balkovsky, E. and Shraiman, B. (2002). Olfactory search at high reynolds number. *Proc. Nat. Acad. Sci.*, 99:12589–12593.

Consi, T., Grasso, F., Mountain, D., and Atema, J. (1995). Explorations of turbulent odor plumes with an autonomous underwater robot. *Biol. Bull.*, 189:231–232.

Duchamp-Viret, P., Chaput, M., and Duchamp, A. (1999). Odor response properties of rat olfactory receptor neurons. *Science*, 284:2171–2174.

Gardner, J. and Bartlett, P. (1999). Electronic noses. *Oxford University Press.*

Grasso, F. (2001). Invertebrate-inspired sensory-motor systems and autonomous, olfactory-guided exploration,. *Biol. Bulletin*, 200:160–168.

Grasso, F., Dale, J., Consi, T., Mountain, D., and Atema, J. (1997). Effectiveness of continuous

bilateral sampling for robot chemotaxis in a turbulent odor plume: implications for lobster chemo-orientation. *Biol. Bull.*, 193:215–216.

Hayes, A., Martinoli, A., and Goodman, R. (2002). Distributed odor source localization. *IEEE Sensors*, 2:260–271.

Hopfield, J. (1995). Pattern recognition computation using action potential timing for stimulus representation. *Nature*, 37:33–36.

Hugues, E., Rochel, O., and Martinez, D. (2003). Navigation strategies for a robot in a turbulent odor plume using bilateral comparison. *International Conference on Advanced Robotics (ICAR), June 30 - July 3, University of Coimbra, Portugal.*

Ishida, H., Kobayashi, A. Nakamoto, T., and Moriizumi, T. (1999). Three-dimensional odor compass. *IEEE Trans. Robot. Autom.*, 15:251–257.

Ishida, H. and Moriizumi, T. (2003). Machine olfaction for mobile robots. *Chapter 16 in the Handbook of Machine Olfaction Edited by T.C. Pearce, S.S. Schiffman, H.T. Nagle and J.W. Gardner*, pages 399–418.

Kraus-Epley, K. and Moore, P. (2002). Bilateral and unilateral antennal lesions alter orientation abilities of the crayfish, *orconectes rusticus. Chem. Senses*, 27:49–55.

Lilienthal, A. and Duckett, T. (2003). Experimental analysis of smelling braitenberg vehicles. *International Conference on Advanced Robotics (ICAR), June 30 - July 3, University of Coimbra, Portugal.*

Lilienthal, A., Ulmer, H., Fröhlich, H., Stützle, A., Werner, F., and Zell, A. (April 26 - May 1,

2004). Gas source declaration with a mobile robot. *Proceedings of the IEEE International Conference on Robotics and Automation (ICRA 2004), New Orleans, USA*, pages 1430–1435.

Lysetskiy, M., Lozowski, A., and Zurada, J. (2002). Temporal-to-spatial dynamic mapping, flexible recognition, and temporal correlations in an olfactory cortex model. *Biol. Cybern.*, 87:58–67.

Margrie, T. and Schaefer, A. (2003). Theta oscillation coupled spike latencies yield computational vigour in a mammalian sensory system. *Journal of physiology*, 546:363–374.

Marques, L., Nunes, U., and de Almeida, A. (2002). Olfaction-based mobile robot navigation. *Thin Solid Films*, 418:51–58.

McMahon, A., Patullo, B., and Macmillan, D. (2005). Exploration in a t-maze by the crayfish cherax destructor suggests bilateral comparison of antennal tactile information. *Biological bulletin*, 208:183–188.

Nakamoto, T., Ishida, H., and Moriizumi, T. (1996). An odor compass for localizing an odor source. *Sensors and actuators B*, 35-36:32–36.

Pearce, T., Schiffman, S., Nagle, H., and Gardner, J. (2003). Handbook of machine olfaction, electronic nose technology. *Wiley-Vch*.

Porat, B. and Nehorai, A. (1996). Localizing vapor-emitting sources by moving sensors. *IEEE Trans. Signal Processing*, 44:1018–1021.

Rajan, R., Clement, J., and Bhalla, U. (2006). Rats smell in stereo. *Science*, 311:666–670.

Roberts, P. and Webster, D. (2002). Turbulent diffusion. *in Environmental fluid mechanics,*

theories and applications, edited by H. Shen, A. Cheng, K.-H. Wang, M. H. Teng, and C. Liu, ASCE Press, Reston, Virginia.

Russel, R. (1999). Odour detection by mobile robots. *World Scientific Series in Robotics and Intelligent Systems*, 22.

Webster, D., Rahman, S., and Dasi, L. (2001). On the usefulness of bilateral comparison to tracking turbulent chemical odor plumes. *Limnol. Oceanogr.*, 46:1048–1053.

Webster, D. and Weissburg, M. (2001). Chemosensory guidance cues in a turbulent chemical odor plume. *Limnol. Oceanogr.*, 46:1034–1047.

Weissburg, M. (2000). The fluid dynamical context of chemosensory behavior. *Biol. Bull.*, 198:188–202.

Weissburg, M., Dusenbery, D., Ishida, H., Janata, J., Keller, T., Roberts, P., and Webster, D. (2002). A multidisciplinary study of spatial and temporal scales containing information in turbulent chemical plume tracking. *Environ. Fluid Mech.*, 2:65–94.

Yamanaka, T., Ishida, H., Nakamoto, T., and Moriizumi, T. (1998). Analysis of gas sensor transient response by visualizing instantaneous gas concentration using smoke. *Sensors and Actuators A*, 69:77–81.
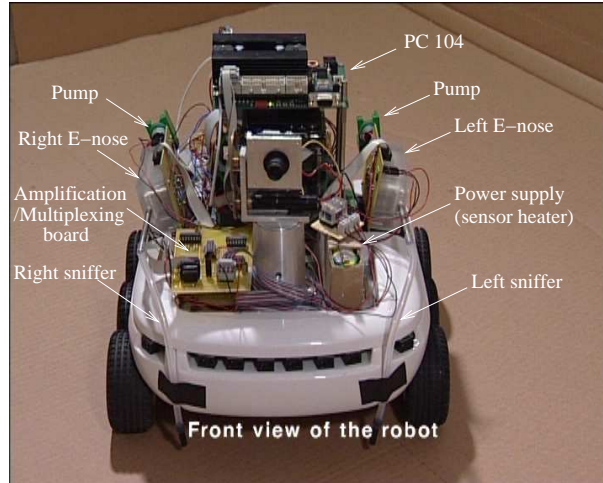
A

B   C

Figure 1: **Olfactory robot**. (A) A Koala robot from k-team was equipped with two electronic noses (E-noses). Two inlet pipes (sniffers), separated by 18 cm, allow to sample the surrounding atmosphere in front of the robot (at the left and right) and two pumps feed the gas directly to the sensors in each E-nose. Data multiplexing, acquisition and processing is performed on the robot. (B) Each E-nose consists of a plexiglas chamber that encompasses a sensor array of ten metal-oxide sensors. (C) These sensors are commercialized with a cap that has a flame-proof stainless steel gauze. In order to improve their response time, the cap was removed from all the sensors in the array.
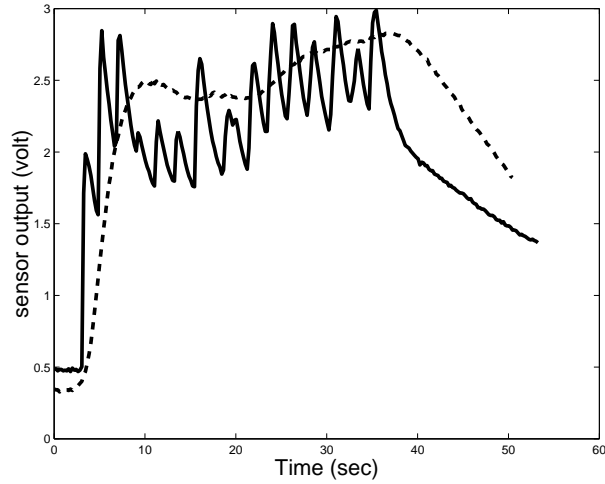
Figure 2: **Effect of the cap on the sensor response**. The dashed curve is the response of a gas sensor (TGS 2620) with the cap. The plain curve is the response of the same sensor without the cap. The fluctuations in the source concentration are the same in the two conditions. These fluctuations are not reflected in the dashed curve because it takes tens of seconds for the response of the sensor with the cap to reach a steady state.

Figure 3: **Olfactometer**. The gas delivery system for *calibration method 1* consists of two micro-pumps (Diaphragm pumps from Sercom 2002 0.35 l/min), two airflow controllers (Tylan mass flow controllers 2900), one bubbler and a data acquisition system (the robot).
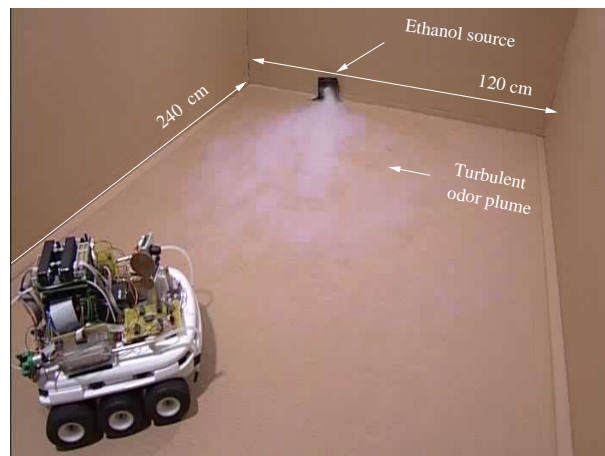
Figure 4: **Experimental arena**. The experiments were performed in an arena of 240 cm long by 120 cm large. An ethanol source was placed at $x = 240$ and $y = 90$ and released at a low rate of 0.35 l/min. To get a turbulent plume, advection is created by a fan placed just behind the source.
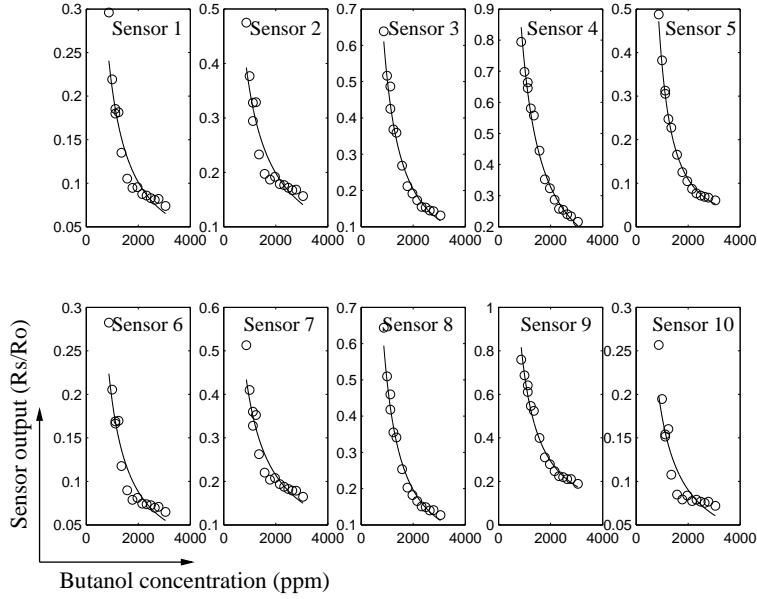
Figure 5: **Calibration method 1**. The different panels (from sensor 1 at the top left to sensor 10 at the bottom right) show the fitted steady state responses R_s/R_o of the ten sensors in the array versus the concentration in butanol (15 different concentrations taken in the range 700-3000 ppm). R_s and R_o is the resistance obtained in presence of the gas and the air, respectively. The array is the E-nose at the left of the robot. The fits are obtained with the power law model (Eq. 1).
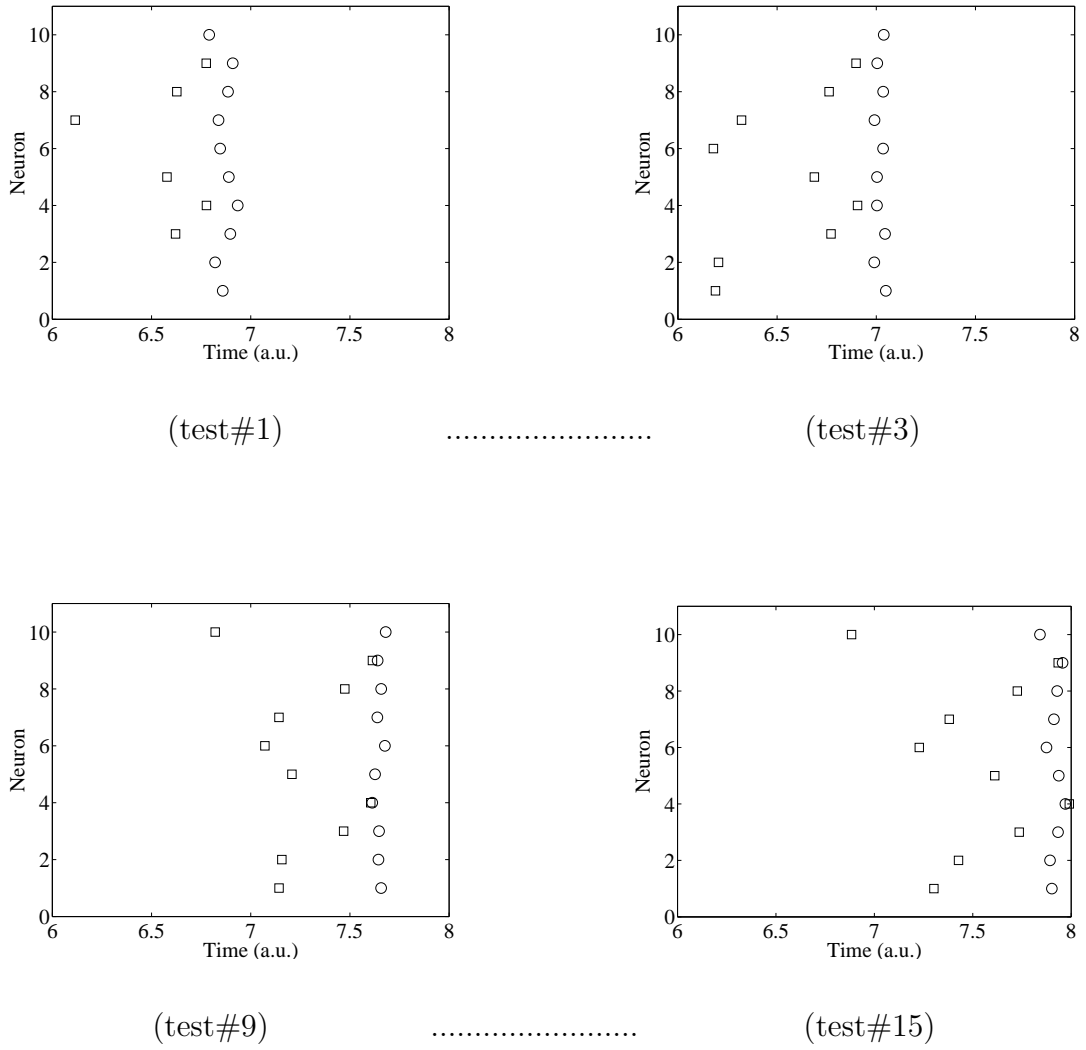
(test#1) .... (test#3)

(test#9) .... (test#15)

Figure 6: **Butanol detector**. The different panels show the arrival times of the spikes fired by the input neurons in presence of butanol (circles) and ethanol (squares). Odor concentration increases from test #1 to test #15. For each test, the concentration of ethanol is similar to the one of butanol.
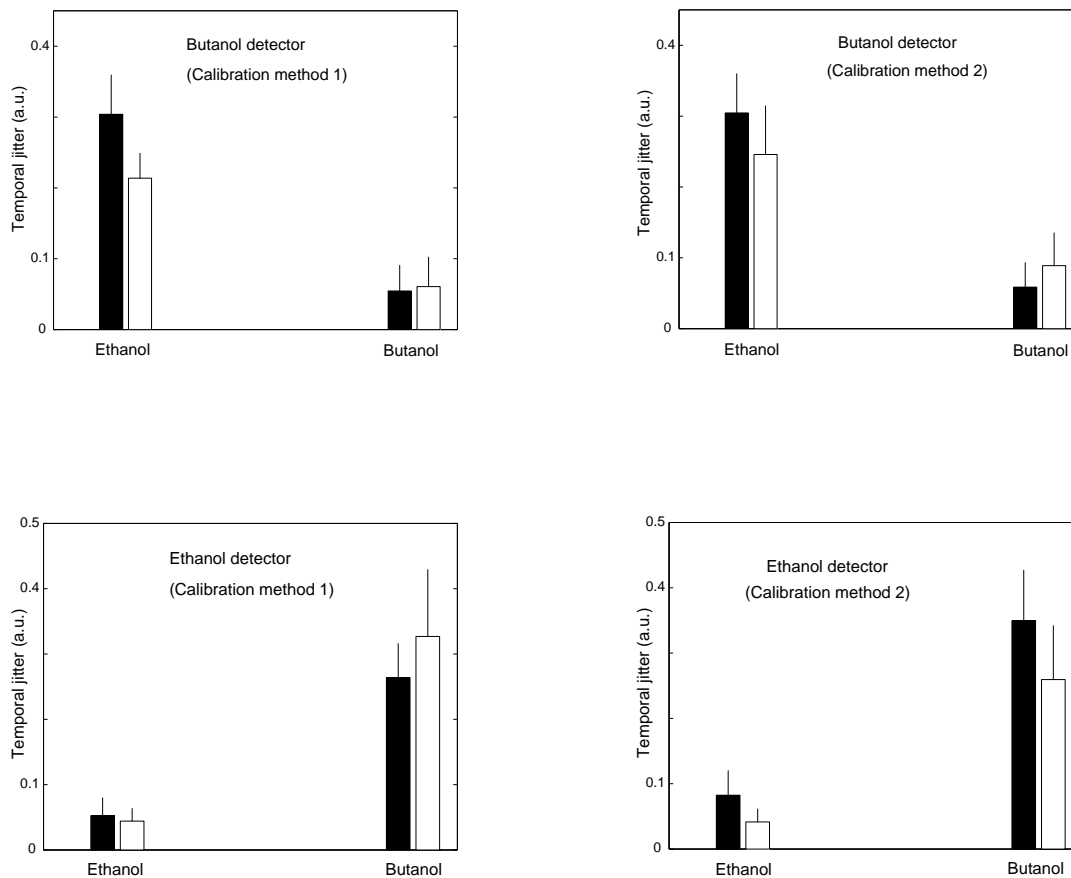
Figure 7: **Performance of the Butanol and Ethanol detectors, for the two calibration methods, and for the two E-noses on the robot**. The different plots show the temporal jitter of the spikes received by the output neuron (butanol or ethanol detector). The black and white histograms are for the E-nose at the left and at the right of the robot, respectively. The error bar represents one standard deviation, estimated as the average over the temporal jitters obtained on the 15 different concentrations of butanol and ethanol.
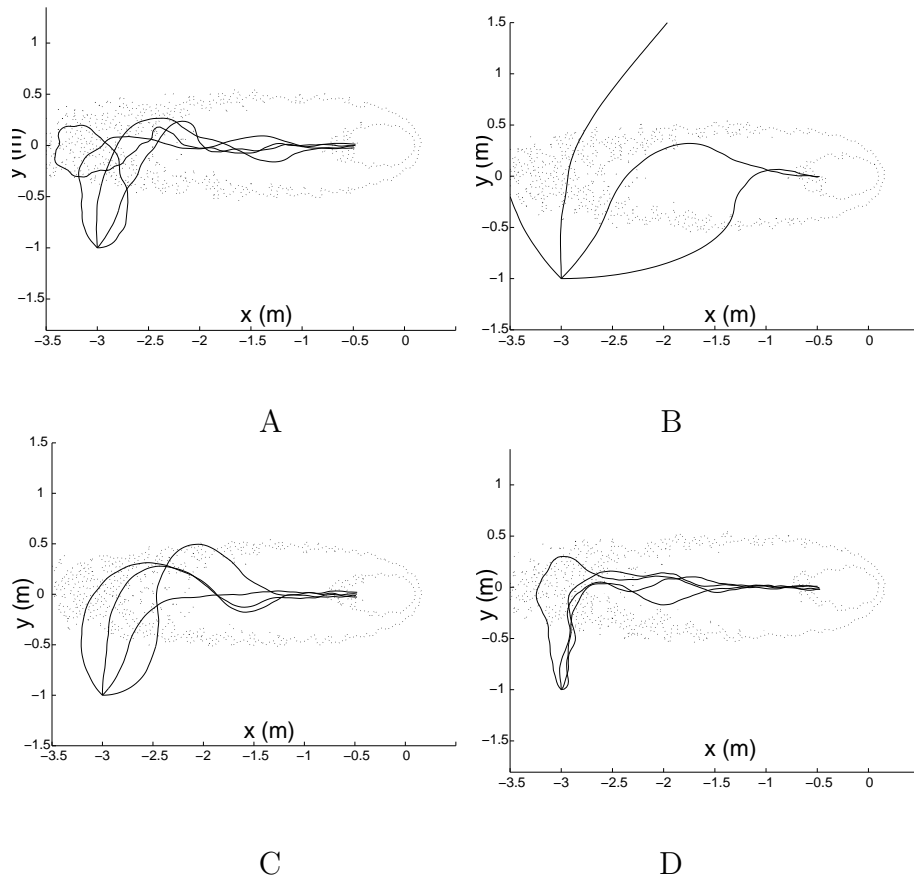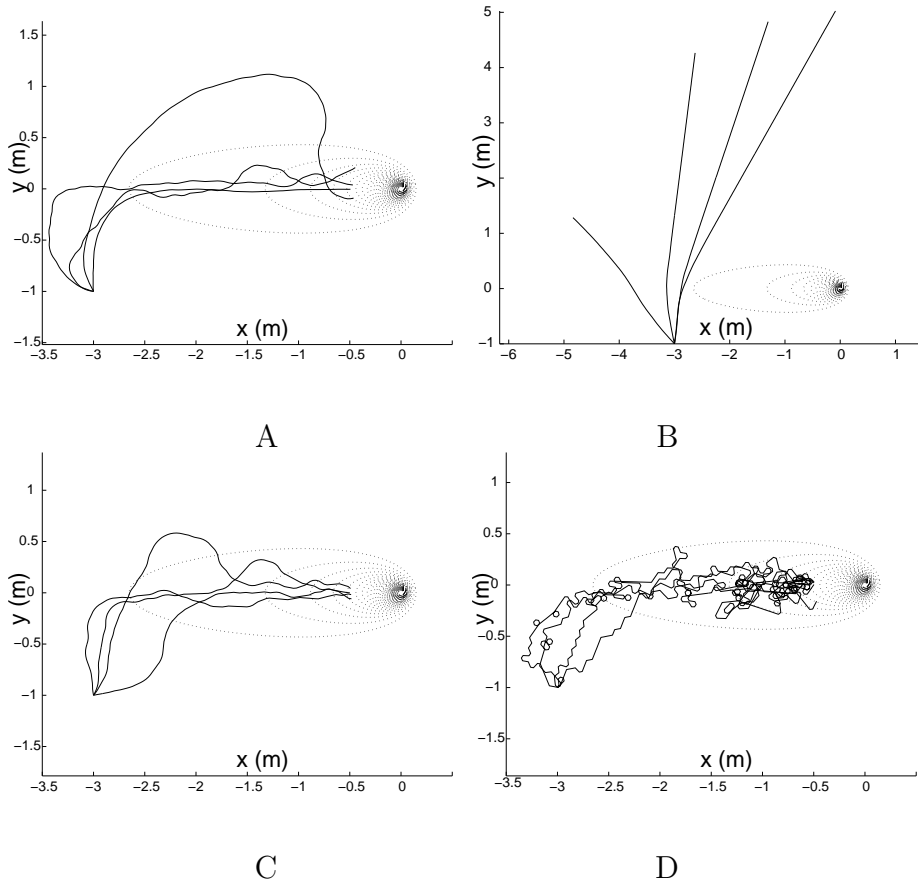
Figure 8: **Simulation of the navigation laws (noisy condition NC1).** Sample trajectories starting from different initial angles for the different navigation laws in the noisy condition NC1 (multiplicative noise of standard deviation $\sigma = 0.2$). The odor source is at (0,0). Wind is in the x-direction from right to left. Panel A is for the binary navigation law. Panels from B to D are for the the analog navigation laws, $\mathcal{L}_0$, $\mathcal{L}_{1/2}$ and $\mathcal{L}_1$.

Figure 9: **Simulation of the navigation laws (noisy condition NC2)**. Sample trajectories starting from different initial angles for the different navigation laws in the noisy condition NC2 (probability of left-right inversion $p = 0.3$). The odor source is at $(0,0)$. Wind is in the x-direction from right to left. Panel A is for the binary navigation law. Panels from B to D are for the the analog navigation laws, $\mathcal{L}_0$, $\mathcal{L}_{1/2}$ and $\mathcal{L}_1$.
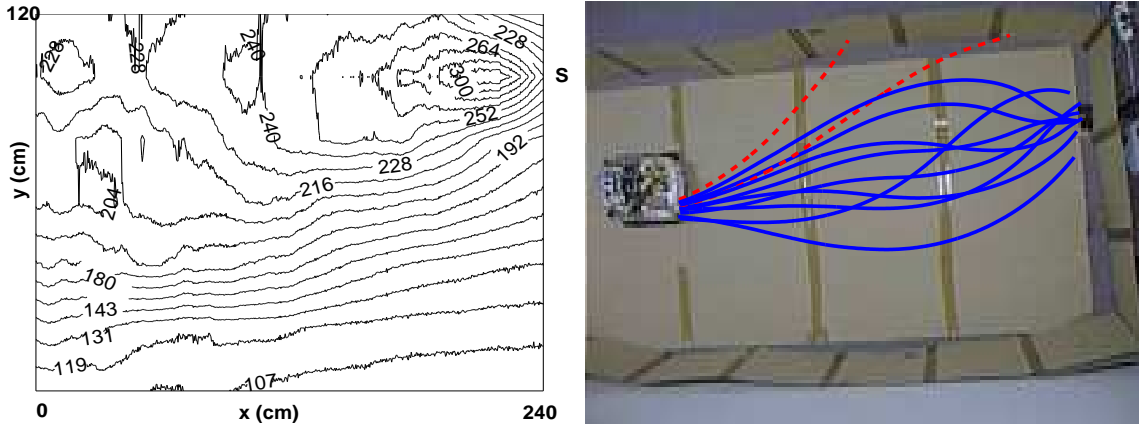
Figure 10: **Robotic experiments.** Left: Contour plot of the spatial distribution of a sensor response in presence of the released gas. This distribution has been obtained by scanning the arena with the robot moving at 2.5 cm/sec. The contour plot was obtained by linear interpolation between neighboring measurement points and the indicated values on the contours represent the obtained sensor responses (quantized with 10 bits) between 0 and 1024. The arena is 240 cm long by 120 cm large. The ethanol source (S) is at $x = 240$ and $y = 90$. Wind is in the x-direction from right to left. Right: Successful trajectories (full lines) and unsuccessful trajectories(dashed lines) of the robot starting from the same location ($x = 70$ and $y = 70$).
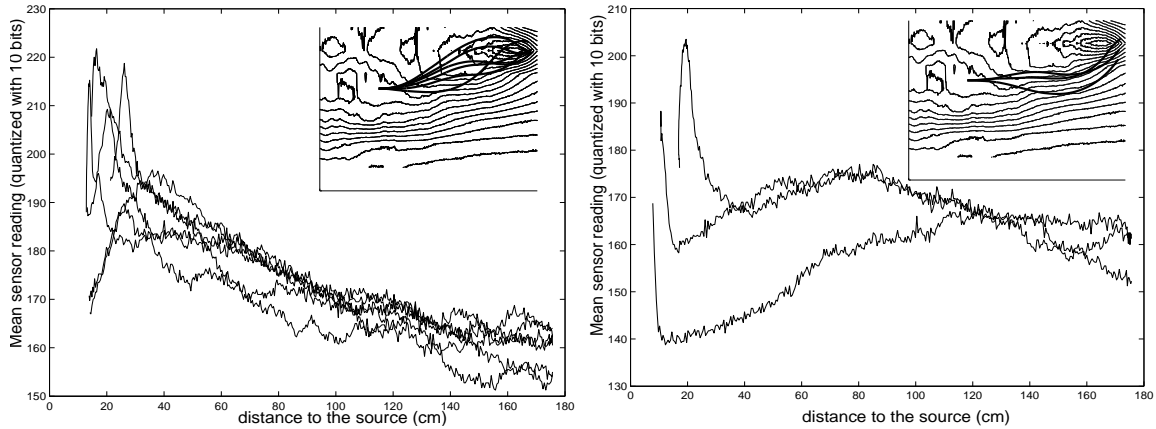
Figure 11: **Mean sensor reading versus distance to the source during the successful robot trajectories.** Two types of trajectories have been found, those for which the sensor reading increases during the path towards the source (figure at the left) and those for which the sensor reading does not always increase (figure at the right). Insets in the figures represent the corresponding trajectories.